ELSEVIER

Journal of Alloys and Compounds 327 (2001) 87–95

Journal of ALLOYS AND COMPOUNDS

www.elsevier.com/locate/jallcom

In situ characterization of phase transitions in cristobalite under high pressure by Raman spectroscopy and X-ray diffraction

V.B. Prokopenko[a,*], L.S. Dubrovinsky[a], V. Dmitriev[b], H.-P. Weber[b]

[a]*Department of Earth Science, Uppsala University, S-752 36 Uppsala, Sweden*
[b]*Swiss–Norwegian Beam Line, SNBL/ESRF, PO Box 220, F-38043 Grenoble, France*

Received 10 January 2001; accepted 10 April 2001

Abstract

We have studied, in situ, the structure and optical properties of cristobalite under non-hydrostatic pressures of up to 61 GPa by means of micro-Raman spectroscopy and X-ray powder diffraction. The starting material, the α-cristobalite phase of SiO_2 (C-I), was formed after annealing of silica sol-gel glass at 1500°C for 15 min. Mao-Bell and membrane-type diamond anvil cells were used for generation of the high pressure. On increasing the pressure, four polymorphs were found: C-I α-cristobalite up to 6 GPa, C-II in the pressure range 0.2–14 GPa, C-III from 14 to 35 GPa, and C-IV above 35 GPa, and no new phase was observed up to 61 GPa. The high-pressure phase C-IV is crystalline and quenchable. A monoclinically distorted α-PbO_2-type structure provides the best fit to the X-ray powder pattern of the recovered phase C-IV.

Keywords: Inorganic materials; Crystal structure; X-ray diffraction; High pressure; Raman spectroscopy

1. Introduction

Silica is an industrially important and widely used material [1]. The study of the high-pressure behavior of different phases of silica plays a significant role for modeling processes in the deep interior of the Earth [2]. There are a number of publications on the high-pressure behavior of α-quartz, stishovite, coesite and amorphous silica summarized in Ref. [3]. Cristobalite, as one of the tectosilicate minerals and a high-temperature polymorph of silica, has attracted much less attention so far.

A series of phase transitions have been reported on the cold compression of α-cristobalite. X-ray, Raman and IR studies documented a phase transition from tetragonal to a lower-symmetry monoclinic phase at ~1.5 GPa [4–7]. At pressures >10 GPa, several groups [6–10] have reported a phase transition to one more phases: phase XI according to Ref. [8], and cristobalite III according to Ref. [3] (although they recognized the structure, these phases may differ considerably from cristobalite). Under quasi-hydrostatic conditions, a structure very similar to that of stishovite was formed above ~20 GPa [10]. Phase XII or cristobalite IV was found to exist on further compression of α-cristobalite above 40 GPa [8,9]. On decompression of phase XII, a new polymorph known as phase XIII was synthesized. Not much is known about the nature and the structure of all phases 'X' [3,9]. For the same pressure range (i.e. >10 GPa), there are some reports on the amorphization of α-cristobalite [7,11,12] and the relation between amorphization and the phase transitions mentioned above is still unclear. The effect of hydrostaticity on the phase transformation of cristobalite has been described [10]. In addition to the diffraction lines of phase XIII [8], extra lines have been observed [6,9,10]. The intensity of these lines decreases with increasing time of exposure at high pressure and at least more than 11 days are required to obtain a single XIII phase.

Since several names are used in the literature [3–10] for the high-pressure polymorph of cristobalite, in this paper we will follow the notation introduced by Hemley et al. [3], i.e. cristobalite I, II, etc. or more simply C-I, C-II, etc. The letter 'C' in the name of the phases (or a mixture of different phases appearing at a certain pressure) described here indicates that a certain high-pressure material(s) was formed from cristobalite as a starting phase. The symbol 'C' does not relate to the structure of the material. The reason for introducing the symbol 'C' is that structures of high-pressure metastable phases and the conditions of their formation depend on the structure of the starting material

*Corresponding author.
E-mail address: vitali.prokopenko@geo.uu.se (V.B. Prokopenko).

0925-8388/01/$ – see front matter
PII: S0925-8388(01)01402-5

(e.g. quartz, stishovite, coesite, tridymite, cristobalite, glass, etc. give different phases on compression). To distinguish the different phases of silica that can be obtained from different starting materials we propose to use letters in the phases' names.

The purpose of this work was to study the in situ phase transformations of cristobalite under non-hydrostatic compression in diamond anvil cells using two different methods — micro-Raman spectroscopy and X-ray powder diffraction.

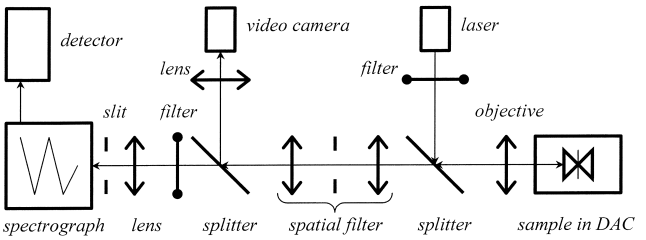

Fig. 2. Optical setup with confocal micro-system for collecting Raman spectra at high pressure in DAC.

2. Experimental

2.1. Sample synthesis

Samples of cristobalite (C-I) were synthesized using the sol-gel technique [13]. A schematic diagram of the sol-gel process is shown in Fig. 1. A precursor solution was prepared by mixing tetraethoxysilane (TEOS), water and hydrochloric acid in the mole ratio 1:25:0.05, respectively. A finely dispersed silica powder (aerosil A-300, SiO_2 particles ~10 nm in diameter) was added to the sol (molar ratio TEOS/SiO_2 1:1) followed by ultrasonic dispersion and separation of the solid remnant by centrifugation. The pH of the sol was increased to 6–7 by the addition of ammonia solution to promote the gelation process. The sol was then poured into closed polystyrene containers and left for 1 day for gelation. After drying at 60°C for 72 h the silica xerogel was heated to 1200°C at a rate of 100°C/h. A transparent amorphous silica was obtained. The cristobalite phase of SiO_2 was formed after annealing the sol-gel glass at 1500°C for 15 min and then grinding to obtain a microcrystalline powder with a particle size of about 1 μm.

According to X-ray diffraction and Raman spectroscopy, pure tetragonal α-cristobalite (lattice parameters a = 4.9658(7) Å and c = 6.9140(9) Å) was prepared using the sol-gel technique and was used as starting material.

2.2. High-pressure technique

Mao-Bell and membrane-type diamond anvil cells (DACs) were used for high-pressure experiments. No pressure medium was used, which implies non-hydrostatic conditions.

Type I brilliant cut diamond anvils with 300 μm culets were used. Holes of 130 μm diameter were drilled into 300 μm thick stainless steel or Re gaskets pre-indented to a thickness of 40–50 μm.

The Mao-Bell DAC was used for in situ micro-Raman spectroscopy and X-ray powder diffraction at the Uppsala Laboratory (Sweden) for three different sets of compression/decompression experiments with maximum pressures of 30, 40 and 61 GPa. Pressure was measured by a ruby scale with an accuracy of ±2%.

Membrane-type DAC was used for X-ray powder diffraction measurements up to 56 GPa at the European Synchrotron Radiation Facility (Grenoble, France, beam line BM01). A gold wire 10 μm in diameter was placed in the pressure chamber and served as internal pressure standard. The accuracy of the pressure measurements was ±1 GPa at the maximum pressure (56 GPa) reached.

Raman spectroscopy was carried out on all quenched samples. Good reproducibility for all series was obtained.

2.3. Analytical technique

Raman spectra were recorded with an InstaSpec-IV CCD detector operating with a MultiSpec-257 imaging spectrograph (grating 1200/350). A confocal micro-optical system in backscattering geometry was used (Fig. 2) [14]. For Raman excitation we used the green line of an argon laser (λ = 514.53 nm). The output power energy of the laser beam was varied in the range 100–350 mW and focused to a spot of about 6 μm in diameter on the sample

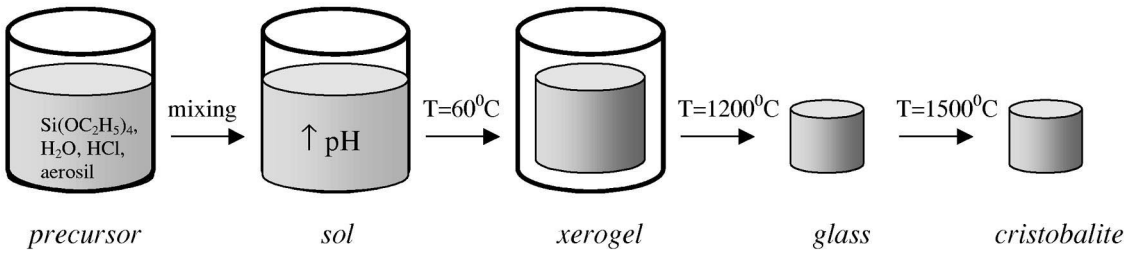

Fig. 1. Schematic diagram of the preparation of cristobalite using the sol-gel technique.

in the DAC. Raman scattering was recorded in the spectral range 180–2800 cm^{-1} with a resolution of 4 cm^{-1}.

At the Uppsala Laboratory we obtained powder X-ray diffraction data with a Siemens X-ray system consisting of a Smart CCD Area Detector and a direct-drive rotating anode as X-ray generator (18 kW). Mo Kα radiation (tube voltage 50 kV, tube current 24 mA, cathode gun 0.1×1 mm^2) was focused with a capillary X-ray optical system to a diameter of 40 μm FWHM. The diffracted X-rays were collected on a 512×512 pixel area detector. Data were acquired in different experiments at different fixed 2θ settings of 5, 12, 20 and 25° (corresponding to the fixed positions of the detector) and by varying the sample-to-detector distance (170–260 mm). Settings of the detector were carefully calibrated using three independent standards (Pt, Au and Re) at each position of the detector. Since a large portion of the Debye rings are measured on the detector surface, it reduces the counting time by the solid angle covered. The collection times were 3 to 12 h.

The monochromatic radiation from the third generation synchrotron at ESRF permits the investigation of samples of very small size with area detectors. At ESRF (beam line BM01) powder diffraction data were collected with a MAR345 detector using an X-ray beam of 0.6996 Å wavelength and a size of 55×55 μm^2. The collected images were integrated using the Fit2D program in order to obtain a conventional diffraction spectrum [15].

All recorded spectra were analyzed using Origin 6.0 software and backgrounds were subtracted from smoothed curves.

3. Results

3.1. Micro-Raman spectroscopy

Fig. 3 shows selected Raman spectra (RS) of cristobalite on increasing the pressure to 61 GPa. A new Raman peak located at 485 cm^{-1} appears at a pressure of 0.2 GPa. On increasing the pressure the position of this band shifts to 530 cm^{-1} at 6.3 GPa and its intensity also gradually increases. Above 2.2 GPa, two new peaks located at 245 and 640 cm^{-1} are observed. The Raman peaks from the initial α-cristobalite phase disappear at 6.3 GPa and the transition from phase C-I to C-II is completed.

A few weak lines from a second high-pressure phase C-III appear at 14 GPa and the intensities of the peaks of phase C-II decrease (Fig. 3a). The Raman modes of phase C-III reach a maximum intensity at 28 GPa and are characterized by a number of strong and sharp peaks (214, 325, 389, 486, 533, 581, 681, and 757 cm^{-1}). Above 31 GPa, the Raman spectra of C-III display decreasing intensity and broadening of the peaks. At 35 GPa, new Raman modes appear and at 40 GPa only the peaks from

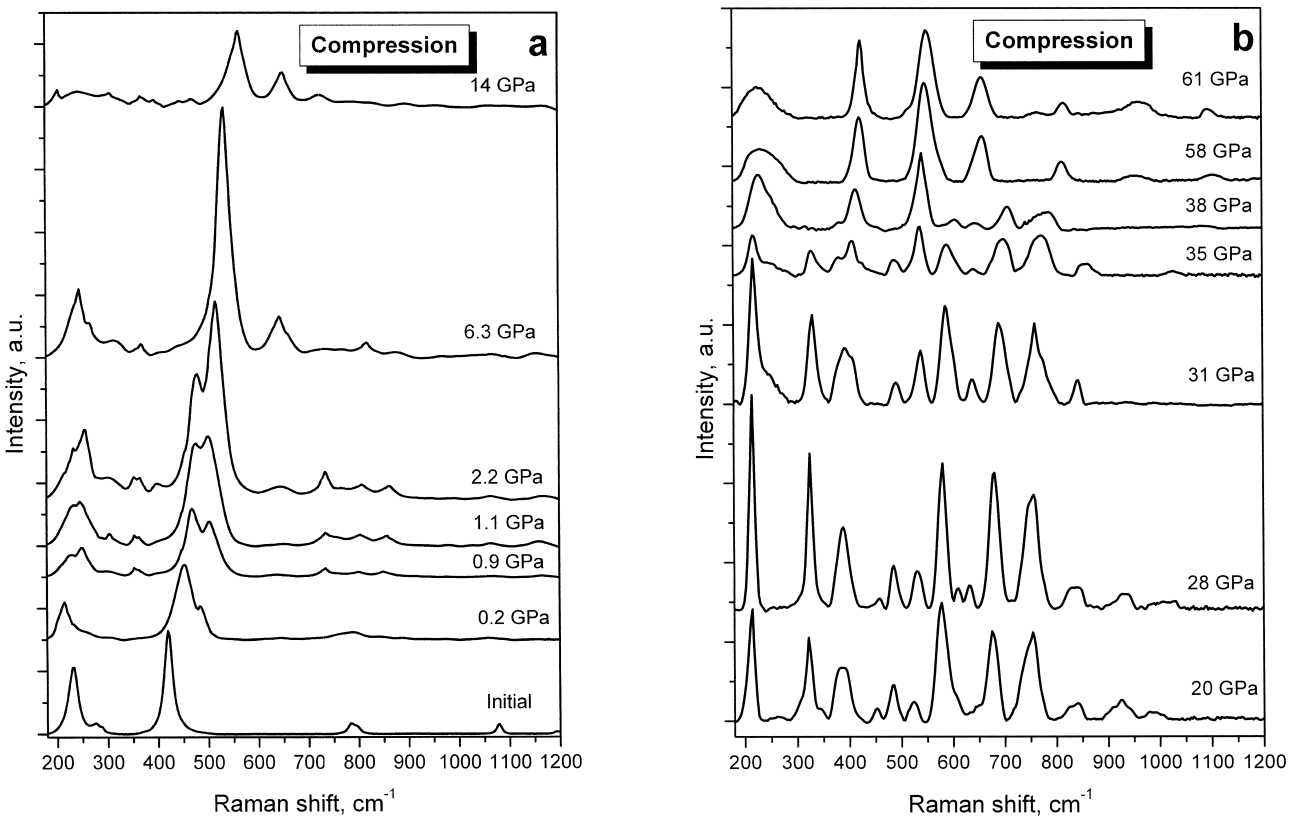

Fig. 3. Raman spectra collected on compression of α-cristobalite to 14 GPa (a) and to 61 GPa (b).

new phase C-IV are present. Increasing the pressure further to 61 GPa does not lead to any significant changes in the RS except for shift of the peaks. At 61 GPa the high-pressure polymorph C-IV of silica is characterized (Fig. 3b) by three intense and comparably narrow peaks located at 425, 554 and 664 cm^{-1}. One broad low-frequency Raman band at 245 cm^{-1} and a few weak and broad Raman bands at 818, 960 and 1080 cm^{-1} for phase C-IV were also observed (Fig. 3b).

The small size of the laser spot (diameter ~6 μm) and the confocal setup of the Raman spectrometer allowed us to study the radial distribution of the material across the pressure chamber by following the variation in pressure from the center of the hole towards the gasket. Micrometer sized ruby chips were used to measure the pressure at each point.

It was found that, at all pressures up to 61 GPa, the central regions, at least 60 μm in diameter (130 μm sample chamber diameter), have the same pressure and identical RS as described above. Near the gasket, the pressure decreased by 30–50% (depending on the peak pressure) and the RS changed correspondingly. For example, at 40 GPa in the central area of the sample, the pressure decreased to 20 GPa at the gasket border. The variations in the RS recorded at 40 GPa peak pressure from the center of the sample chamber towards the gasket border are illustrated in Fig. 4. We observed that, under such conditions, both C-IV and C-III polymorphs are present in the same pressure chamber. However, at 61 GPa peak pressure, only the high-pressure phase C-IV was found.

On reducing the pressure (Fig. 5) from 61 GPa the positions of the two most intense Raman bands (425 and 554 cm^{-1} at 61 GPa) of high-pressure cristobalite polymorph C-IV shifted to low frequency and their intensity did not change significantly. For the quenched sample these lines had a very sharp shape below 2.5 GPa and were located at 378 and 514 cm^{-1}, respectively. The low-frequency peak (425 cm^{-1}) was broadened and even split at pressures between 23 and 12 GPa (Fig. 5). At 23 GPa, several new features appeared — a relatively intense Raman band located at 760 cm^{-1} and weaker peaks at 850, 670 and 620 cm^{-1}. The peak at 760 cm^{-1} weakly depends on pressure and for the quenched sample it has a maximum at 738 cm^{-1} (Fig. 5). This peak becomes sharper on decompression. Such behavior of the Raman spectra could be due to recrystallization, changes in the preferred orientation, or the appearance of an intermediate phase at 23 GPa. The major Raman bands of the high-pressure phase C-IV are present for the quenched sample, but become narrower at low pressure. Besides the sharp peaks discussed above (Fig. 5), several very broad Raman bands with maxima at about 215, 490, 795 and 1080 cm^{-1} are present in the spectrum of the quenched sample.

Unlike the polymorph C-IV of cristobalite, the phase

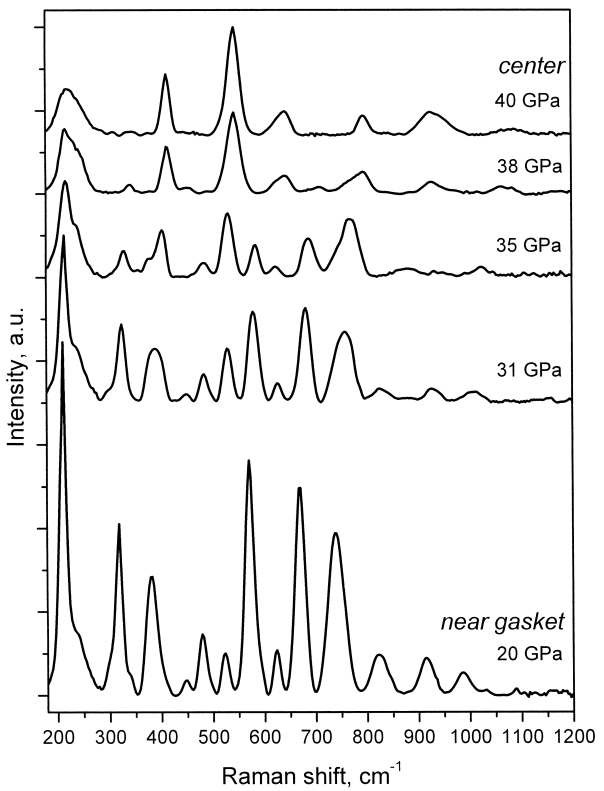

Fig. 4. Raman spectra at a peak pressure of 40 GPa collected at different locations in the pressure chamber.

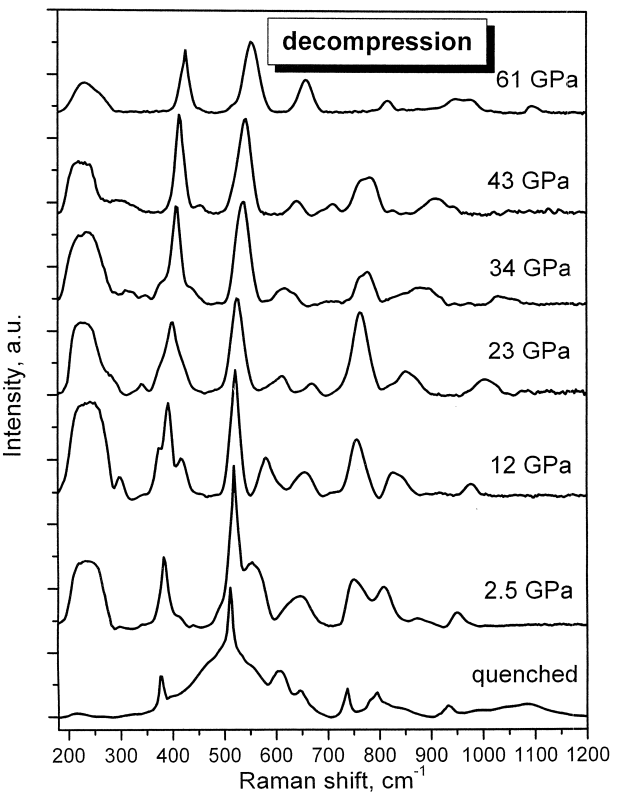

Fig. 5. Raman spectra collected on decompression from 61 GPa.

C-III (i.e. cristobalite compressed up to 20–30 GPa) shows different behavior on decompression. Fig. 6 shows an example of the RS recorded near the gasket on decompression from 20 GPa. On reducing the pressure to 14 GPa the intensity of the low-frequency Raman bands (below 500 cm^{-1}) decrease and their positions shift. Simultaneously, the high-frequency Raman bands also shift to lower-frequency ranges, but the ratio of peak intensities changes and at 8 GPa (Fig. 6) a very intense line is found at 540 cm^{-1} and weaker lines are observed at 625 and 700 cm^{-1}. The shape of the RS at 8 GPa (Fig. 6) is very similar to those observed on increasing the pressure at 14 GPa (Fig. 3) and correspond to a mixture of phases C-II and C-III. However, on further decompression the C-II polymorph was not observed (a reversible phase transition C-I↔C-II was reported in Ref. [7]). The quenched samples exhibited only a few wide Raman bands in contrast to the quenched sample from polymorph C-IV (Figs. 5 and 6).

The variations of the RS recorded for the quenched materials obtained at different peak pressures are shown in Fig. 7. For the samples compressed to a maximum pressure of 20 GPa the most intense broad Raman band is located at about 460 cm^{-1}, while the same band is found at 490 cm^{-1} when the material was decompressed from 40 GPa. For quenched samples decompressed from peak pressure at 35 GPa, new sharp peaks appear (Fig. 7). At pressures of about 35 GPa, two phases, C-III and C-IV, co-exist in the sample (Fig. 3). As a result, two components are present in the material quenched from pressures above 35 GPa (Fig. 7). One component is characterized by a few broad Raman bands with a maximum located at about 480 cm^{-1}, which may correspond to an amorphous silica network, and the second has a number of sharp and narrow peaks from the crystalline phase. At peak pressures above 40 GPa (only phase C-IV is present) the broad Raman band of the quenched sample becomes narrower with decreasing intensity and shifts to 490 cm^{-1}. At the same time the intensity of the sharp peaks increases.

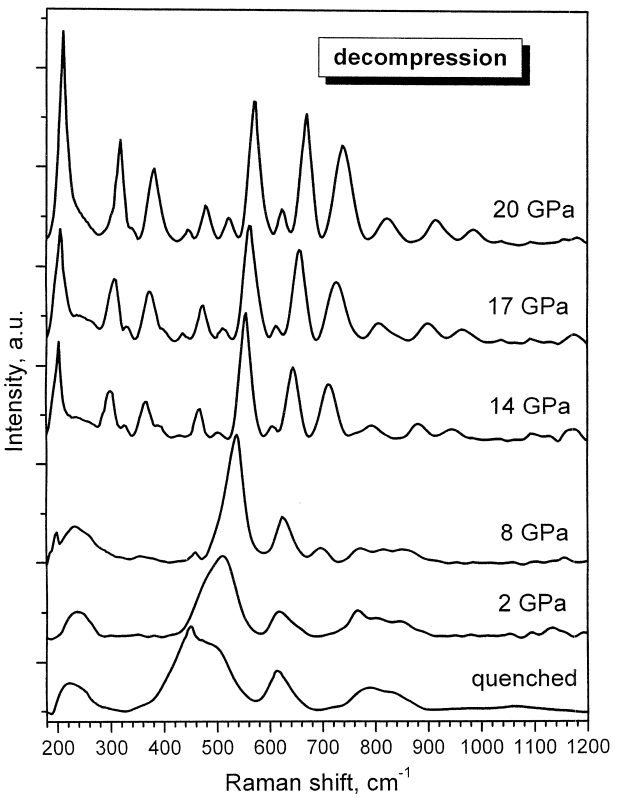

Fig. 6. Raman spectra collected on decompression from 20 GPa.

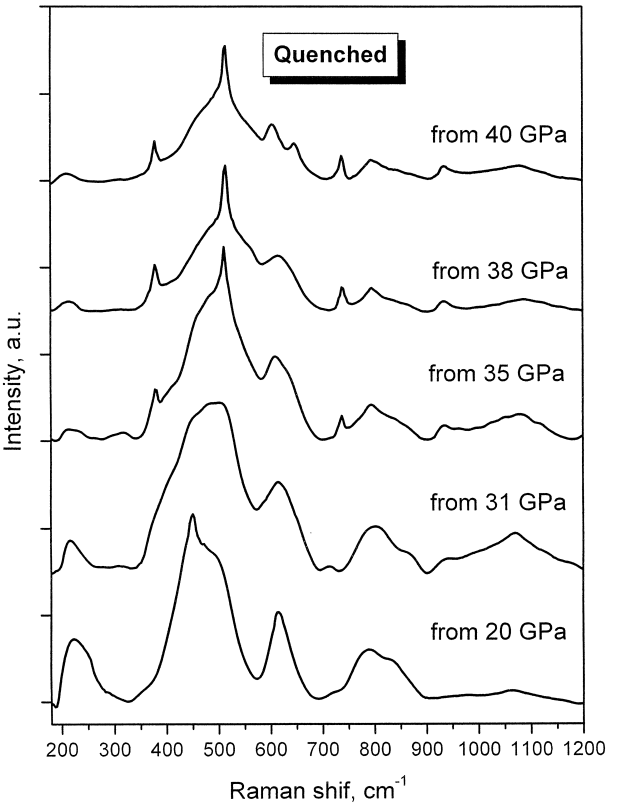

Fig. 7. Raman spectra of quenched samples recovered from different peak pressures.

3.2. X-ray powder diffraction

The sequence of phase transformations of cristobalite at increasing pressure, from C-I to C-IV, observed by Raman spectroscopy was confirmed by X-ray powder diffraction data obtained at the Uppsala Laboratory and at ESRF. Examples of a typical 2D diffraction image obtained at ESRF with a MAR345 area detector and of selected conventional integrated spectra are shown in Figs. 8 and 9, respectively. Diffraction patterns were collected on compression to 56 GPa and after decompression. As starting material, α-cristobalite mixed with Au wire (serving as a pressure calibrant) was used.

Fig. 10 shows the pressure dependence of some interplanar spacings of cristobalite. At 3 GPa (Fig. 10) the intensity of the (101) α-cristobalite reflection drastically

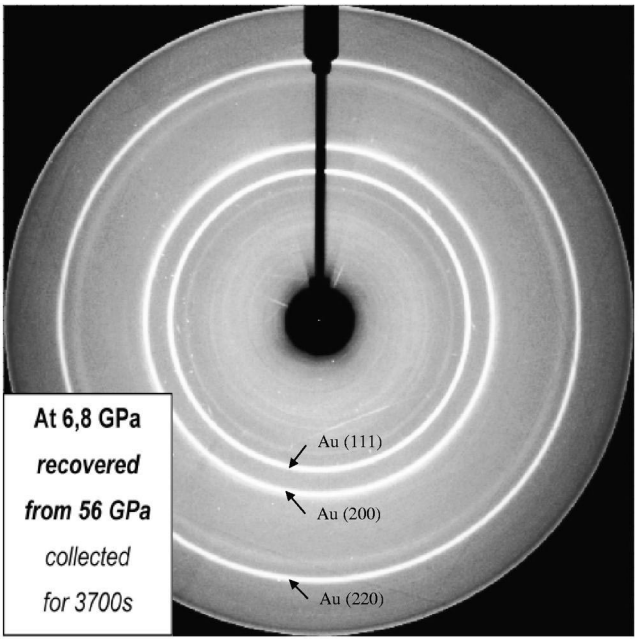

Fig. 8. Example of a two-dimensional diffraction pattern recorded with the imaging plate detector MAR345 for a mixture of cristobalite and Au pressure calibrant at 6.8 GPa after decompression from 56 GPa (ESRF, beamline BM01).

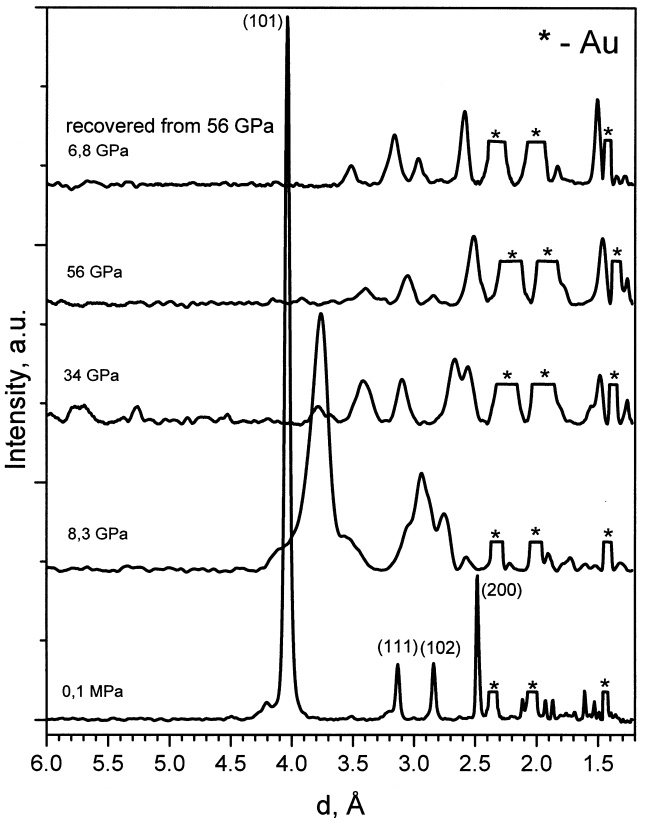

Fig. 9. Integrated diffraction patterns of cristobalite at different pressures.

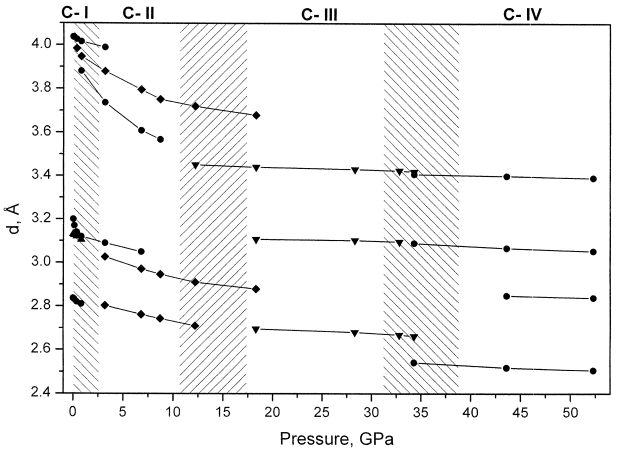

Fig. 10. Pressure dependence of the interplanar spacing of cristobalite.

decreases with simultaneous broadening and splitting of the (111) reflection. At pressures between 5 and 11 GPa the C-II phase is observed (Figs. 9 and 10). This phase is characterized by major reflections of 3.76, 2.94 and 2.76 Å at a pressure of 8.3 GPa. Table 1 shows the lattice parameters of the C-II phase which were calculated using a non-conventional ($p2_1$ group symmetry) monoclinic B-centered cell according to Ref. [4]. From 12 GPa the intensities of the C-II reflections gradually decrease and several new reflections of the phase C-III appear. At pressures of 16 to 28 GPa only the reflections of phase C-III are present. The most intense lines at 28 GPa were located at 3.4, 3.1, 2.7 and 1.49 Å. Above 34 GPa, a new reflection appears at 2.55 Å and after 44 GPa the formation of the high-pressure polymorph C-IV was completed. The major peaks at 56 GPa were located at 3.4, 3.06, 2.84, 2.51 and 1.46 Å. After decompressing to 6.8 GPa these lines shifted to 3.57, 3.16, 2.95, 2.58 and 1.50 Å, respectively. On decompression the relative intensities of the peaks were unchanged. Thus, phase C-IV formed at pressures above 40 GPa is quenchable to 6.8 GPa.

4. Discussion

Fig. 11 shows the variations of the positions of the most intense Raman peaks as a function of pressure. It is clear from the figure that four distinct stages (C-I to C-IV) appear on compression to 61 GPa, in good agreement with earlier observations [3].

It is possible that there is an intermediate phase between C-II and C-III on compression at around 14 GPa (Fig. 3a) and on decompression at around 8 GPa (Fig. 6). However, X-ray diffraction does not provide any evidence for such a phase. This means that the observed peculiarities in the Raman spectra could be associated with the behavior of the disordered silica network or an amorphous component.

Palmer et al. [7] studied in detail the Raman spectra of cristobalite compressed under quasi-hydrostatic conditions

Table 1
Lattice parameters of high-pressure phases C-II and C-IV

Lattice parameters	Monoclinic B-face centred ($p2_1$) [14] C-II phase	Monoclinically distorted α-PbO_2-type (*Pbcn*) C-IV phase	
Pressure	8.3 GPa	56 GPa	Recovered to 6.8 GPa
a (Å)	8.843(1)	4.327(1)	4.381(8)
b (Å)	4.508(1)	3.622(1)	3.781(9)
c (Å)	13.569(3)	5.686(1)	5.918(8)
β (deg)	94.48(7)	91.65(2)	90.2(1)

up to 22 GPa. It was established that cristobalite has two phase transitions: 'cristobalite I↔II' at a pressure of 1.2 GPa, and above 13 GPa 'cristobalite III'. The same phase transitions were observed with X-ray powder diffraction [4]. In general, similar behavior of the RS was observed for cristobalite under non-hydrostatic compression in our study. However, there are some differences. In our study the first peak from the C-II phase appeared at 0.2 GPa (1.4 GPa in Ref. [7]) (Fig. 3a). According to Ref. [7] and our study at 6 GPa, only the C-II phase is present in the sample. However, our RS show an additional Raman peak (Fig. 3a) located at 640 cm^{-1}, which was not reported by Palmer et al. [7]. Above 13 GPa, a new sharp mode, close to 470 cm^{-1}, was reported in Ref. [7], but we did not observe this in our studies in the pressure range 13 to 18 GPa (Fig. 3a). We found that, above 20 GPa, the RS are characterized by a number of sharp and intense lines at 28 GPa close to 214, 325, 389, 486, 533, 581, 681 and 757 cm^{-1} (Fig. 3b), which were not observed in Ref. [7]. These observations can be explained by the differences in the experimental conditions — quasi-hydrostatic in Ref. [7] (a methanol–ethanol–water mixture was used) and non-hydrostatic (no pressure medium) in the present study.

Our Raman studies clearly show that phases C-III and C-IV are significantly different (Fig. 3b). Phase C-III is characterized by three groups of lines. Each group consists of three equally intense lines. Two groups with intense Raman bands are located in the low- and middle-frequency range and one weaker group is located close to the high-frequency range (Figs. 3b and 4). Phase C-IV has only three intense lines in the middle-frequency area. The Raman spectra of C-III and C-IV are clearly distinguishable from the spectra published in Refs. [1,2,7,10]. This means that C-IV and C-III are new silica polymorphs. The same situation holds for the sample quenched from phase C-IV, for which the positions of the sharp RS lines cannot be matched to the RS of known structures of SiO_2.

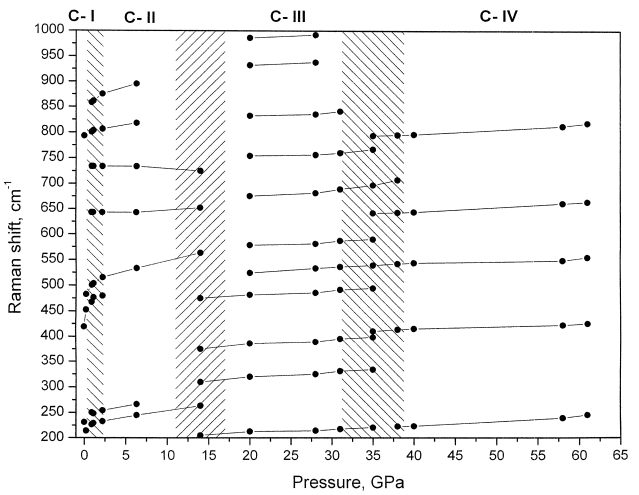

Fig. 11. Pressure dependence of the Raman bands (the solid lines are guides to the eye).

The diffraction pattern of the sample treated at the maximum pressure of 56 GPa and decompressed to 6.8 GPa contains a number of peaks (Figs. 9 and 12) which could correspond to stishovite (Fig. 12e). However, the intense reflections at 3.57, 3.16, 2.95, 2.58 and 1.50 Å could not be assigned to the stishovite structure. This observation is confirmed by Raman spectroscopy data. Similar *d*-spacings were reported by Yagi and Yahagi [8] for the quenched sample recovered from the peak pressure 53.1 GPa: at 3.166, 2.966, 2.595 and 1.494 Å. Later, Yagi et al. [6,9,10] located a reflection at around 3.5 Å for cristobalite in CsI pressure medium compressed to 40 GPa and in argon at 28 GPa.

It is possible to explain the observed diffraction pattern (Fig. 12a) as a mixture of α-PbO_2-type (Fig. 12d) and a disordered monoclinic $P2_1/c$ phase (Fig. 12c, Table 2) [16,17]. However, a single model of the monoclinically distorted α-PbO_2-type structure (Table 1) provides a better description of the positions and relative intensities of the diffraction lines of the silica phase obtained on decompression of the sample from a peak pressure of 56 GPa (Fig. 12b).

5. Summary

Micro-Raman spectroscopy and X-ray powder diffraction were used for the in situ characterization of the high-pressure phase transitions under non-hydrostatic condition starting from α-cristobalite. It was shown that, on compression at ambient temperature, four polymorphs of

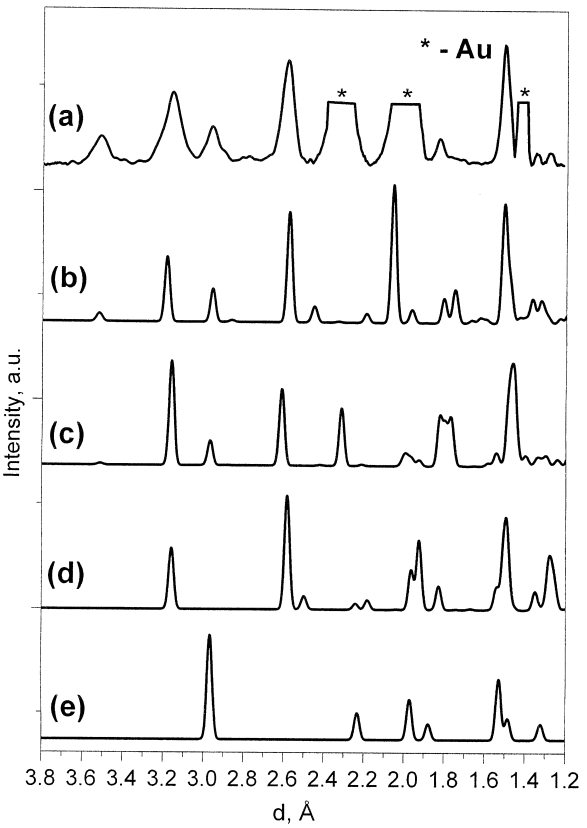

Fig. 12. Comparison of the experimentally observed X-ray powder diffraction pattern of decompressed polymorph C-IV at 6.8 GPa (a) with calculated diffraction patterns of a single model of the monoclinically distorted α-PbO_2-type structure (b), a mixture of α-PbO_2-type and the disordered monoclinic (space group $P2_1/c$) phase proposed in Refs. [16,17] (c), an ideal α-PbO_2-type structure (d) and stishovite (e). Structural information on these high-pressure silica polymorphs used for simulation diffraction patterns are shown in Tables 1 and 2.

cristobalite appeared: C-I (α-cristobalite), C-II in the pressure range 0.2–14 GPa, C-III at pressures between 14 and 35 GPa, and C-IV above 35 GPa. The boundaries between the different phases are fuzzy in the range of ~20% from the middle transition pressure. The Raman spectra of the high-pressure polymorphs C-III and C-IV were recorded here for the first time.

The high-pressure phase C-IV is polycrystalline in contrast to earlier reports [11,12] in which amorphisation of cristobalite above 30 GPa was observed. The Raman spectroscopy data are in good agreement with X-ray data and demonstrate that the phase C-IV is quenchable up to 6.8 GPa and is clearly distinguishable from stishovite or other known silica polymorphs.

Acknowledgements

This work was supported financially by the Swedish Science Foundation (NFR), the Wallenberg and Göran Gustafssons Stiftelse Funds, and Swiss National Science Foundation Grant 21-45702.95. Experimental assistance from the staff of the Swiss–Norwegian beam lines at ESRF is gratefully acknowledged.

References

[1] G.H. Beall, Rev. Miner. 29 (1994) 469.
[2] G. Shen, D.L. Heinz, Rev. Miner. 37 (1998) 369.
[3] R.J. Hemley, C.T. Prewitt, K.J. Kingma, Rev. Miner. 29 (1994) 41.
[4] D.C. Palmer, L.W. Finger, Am. Miner. 79 (1994) 1.
[5] J.B. Parise, A. Yeganeh-Haeri, D.J. Weidner, J.D. Jorgensen, M.A. Saltzberg, J Appl. Phys. 75 (1994) 1361.
[6] Y. Yahagi, T. Yagi, H. Yamawaki, K. Aoki, Solid State Commun. 89 (1994) 945.
[7] D.C. Palmer, R.J. Hemley, C.T. Prewitt, Phys. Chem. Miner. 21 (1994) 481.
[8] Y. Yahagi, T. Yagi, Nature 347 (1990) 267.
[9] M. Yamakata, T. Yagi, Proc. Jpn. Acad. 73B (6) (1997) 85.
[10] T. Yagi, M. Yamakata, in: H. Aoki, Y. Syono, R.J. Hemley (Eds.), Physics Meets Mineralogy, Condensed-Matter Physics in Geosciences, Cambridge, 2000, p. 242.
[11] K. Halverson, G.H. Wolf, EOS Trans. Am. Geophys. Union 71 (1990) 1671.
[12] A.J. Gratz, L.D. DeLoach, T.M. Clough, W.J. Nellis, Science 259 (1993) 663.

Table 2
Structural information for the high-pressure silica polymorphs used for simulation of the diffraction patterns shown in Fig. 12

Lattice parameters	Stishovite		α-PbO_2-type		$P2_1/c$-type					
Space group	$P4_2/mnm$		$Pbcn$		$P2_1/c$					
a (Å)	4.196(8)		4.484(7)		6.674(9)					
b (Å)	–		4.078(6)		4.424(9)					
c (Å)	2.636(7)		4.998(7)		4.625(9)					
β (deg)	–		–		120.1(8)					
Atom	Si	O	Si	O	Si(1)	Si(2)	Si(3)	O(1)	O(2)	O(3)
x	0	0.306	0	0.2576	0.5	0.5	0.16	0.054	0.721	0.387
y	0	0.306	0.1502	0.387	0	0.5	0.521	0.243	0.242	0.237
z	0	0	0.25	0.4201	0	0	0.977	0.651	0.186	0.66
Occupancy	1	1	1	1	0.95	0.25	0.9	1	1	1

[13] V.S. Gurin, V.B. Prokopenko, I.M. Melnichenko, E.N. Poddenezhny, A.A. Alexeenko, K.V. Yumashev, J. Non-Cryst. Solids 234 (1998) 162.
[14] M. Eremets, High Pressure Experimental Methods, Oxford University Press, New York, 1996, pp. 390.
[15] A. Hammersley, Publication No. ESRF98HAO1T, ESRF, 1996.
[16] D.M. Teter, R.J. Hemley, G. Kresse, J. Hafner, Phys. Rev. Lett. 80 (1998) 2145.
[17] J. Haines, J.M. Le'ger, C. Chateau, Phys. Rev. B 61 (13) (2000) 8701.